JOURNAL OF GEOPHYSICAL RESEARCH, VOL. 111, A10215, doi:10.1029/2006JA011654, 2006

Whistler mode illumination of the plasmaspheric resonant cavity via in situ injection of ELF/VLF waves

P. Kulkarni,[1] U. S. Inan,[1] and T. F. Bell[1]

Received 7 February 2006; revised 25 May 2006; accepted 18 July 2006; published 19 October 2006.

[1] Numerical ray tracing indicates that the in situ injection of whistler mode waves of 1 kHz to 4 kHz can be used to illuminate the inner radiation belts and slot region. These results were derived by using the Stanford VLF Ray Tracing Program to simulate sources placed at a total of six points in the inner magnetosphere: $L = 1.5$, $L = 2.0$, and $L = 2.5$ at two geomagnetic latitudes, the equator and a latitude of 20° along each field line. The results demonstrate that an in situ source, by varying the frequency of the injected waves, can illuminate L shells both higher and lower than the source site, with wave frequencies below (above) the local lower hybrid resonance, f_{LHR}, moving to higher (lower) L shells. Accounting for the limitations that would be imposed by a practical antenna immersed in the magnetospheric medium restricts the radiating wave frequency, f, to $0.9\, f_{LHR} \leq F < (f_{LHR} + 1\ \text{kHz})$, and the wave normal angle at injection to no farther than 3° from the resonance cone. Even after accounting for these restrictions, it requires only three in situ sources placed at the above locations to illuminate $1.4 \simeq L \simeq 2.7$, which comprises the bulk of the inner radiation belt.

Citation: Kulkarni, P., U. S. Inan, and T. F. Bell (2006), Whistler mode illumination of the plasmaspheric resonant cavity via in situ injection of ELF/VLF waves, *J. Geophys. Res.*, *111*, A10215, doi:10.1029/2006JA011654.

1. Introduction

[2] Pitch angle scattering of energetic electrons resulting from resonant wave-particle interactions has long been believed to play a significant role in the loss of trapped energetic particles in the near-Earth space environment [*Kennel and Petschek*, 1966; *Lyons et al.*, 1972; *Inan* 1987]. *Abel and Thorne* [1998a, 1998b] recently conducted a comprehensive theoretical study of the loss rates of radiation belt electrons in the 100–1500 keV energy range due to Coulomb collisions and resonant interactions with plasma waves, including plasmaspheric hiss, lightning generated whistlers, and VLF transmitters. Their results documented the substantial impact on electron lifetimes at $L < 2.6$ of VLF transmitters operating continuously in the 17–23 kHz range. Presently, the growing number of satellites vulnerable to enhanced fluxes of relativistic electrons [*Baker*, 2000] has intensified the need to quantify the potential role of anthropogenic effects on the energetic electron population.

[3] It has recently been suggested by *Inan et al.* [2003] that in situ injection of whistler mode waves may be particularly effective at moderating the lifetime of energetic electrons in the inner radiation belt. On the basis of power scaling of the results of the *Abel and Thorne* [1998a, 1998b], this study indicated that a space-borne transmitter radiating frequencies from 1 to 10 kHz can drive diffusion rates that, compared with signals from the ground-based VLF transmitters, may be higher by up to a factor of ~30. It was further noted that lower-frequency waves undergo multiple magnetospheric reflections and thus can be much more efficiently stored in the magnetospheric cavity as compared to the higher wave frequencies from ground-based transmitters [*Inan et al.*, 2003]. In drawing their conclusions, *Inan et al.* [2003] concentrated on waves injected at a single point at $L = 2$ at the magnetic equator and considered only a small number of frequencies and injection wave normal angles.

[4] Before we can fully quantify the potential effects of wave-induced particle precipitation that can be produced by in situ injection of ELF/VLF waves, it is necessary to understand the manner in which electromagnetic wave energy from an in situ source is distributed in the inner magnetosphere. Our purpose in this paper is to expand on the initial results presented by *Inan et al.* [2003] by utilizing the Stanford VLF ray tracing code [*Inan and Bell*, 1977] coupled with an accurate estimation of the path-integrated Landau damping to determine the distribution of wave energy throughout the inner radiation belts based on injection location, wave frequency, and injection wave normal angle. The Stanford VLF ray tracing code models the geomagnetic field as a centered dipole with an electron gyrofrequency of 880 kHz at the ground at the equator and uses the diffusive equilibrium model [*Angerami and Thomas*, 1964] to calculate particle densities. Adopting a different density profile (such as given by *Carpenter and Anderson*

[1]STAR Laboratory, Stanford University, Stanford, California, USA.

0148-0227/06/2006JA011654$09.00

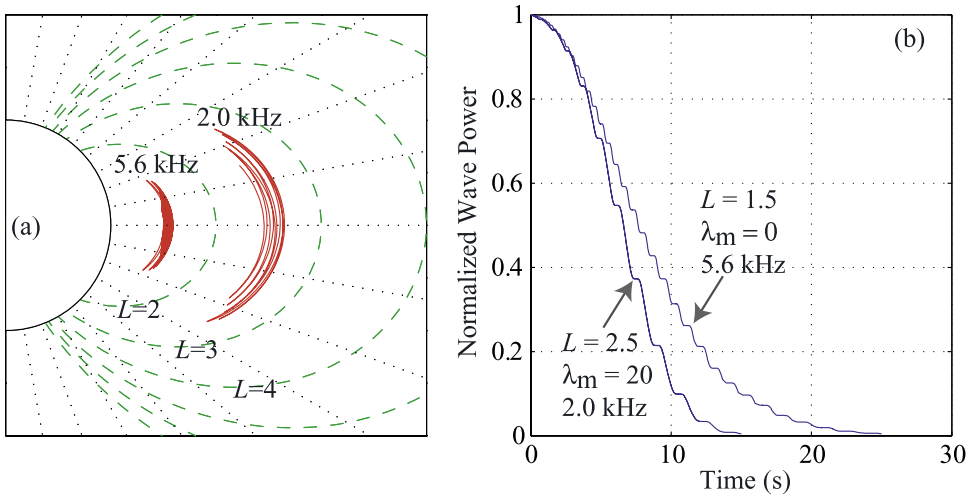

Figure 1. (a) Ray paths of a 5.6 kHz signal injected at $L = 1.5$ at the equator and a 2.0 kHz signal injected at $L = 2.5$ and $\lambda_m = 20$. Both signals were injected at a wave normal angle of $-87°$. (b) Variations of the wave power density (attenuated due to Landau damping) along the ray paths at different L shells. The off-equatorial injection gets attenuated more rapidly.

[1992]) does not significantly change the region of illumination ($\pm 0.2L$) or cavity enhancement factors (± 0.5) for the frequencies considered (see below). For this study we considered a cold, smooth, and uniform plasma without any ducts or density irregularities.

[5] The Stanford VLF ray tracing code has previously been used by *Bortnik et al.* [2003b] to model the frequency-time spectra of lightning-generated magnetospherically reflecting (MR) whistler waves. *Bortnik et al.* [2003b] were able to reproduce the MR whistler spectrogram from *Smith and Angerami* [1968], and they also found agreement with observations made by *Shklyar and Jiříček* [2000] and *Edgar* [1972]. Given the success of the Stanford VLF ray tracing code in modeling MR whistlers, we feel confident in using it to simulate the in situ injection of single frequency VLF waves.

[6] We primarily focus on a single transmitter near the magnetic equatorial plane at $L = 2$ and consider both equatorial and off-equatorial injection points for wave frequencies ranging from well below, to well above, the local lower hybrid resonance (LHR) frequency and also for a broad range of injection wave normal angles. We initially neglect the effects of antenna radiation in a magnetoplasma in order to facilitate a more complete picture of whistler mode wave propagation in the inner magnetosphere as a result of in situ injection. We then modify these results by incorporating the limitations that would be imposed by the *Wang and Bell* [1970] model for a short electric dipole radiating in a magnetoplasma.

2. Magnetospheric Cavity Enhancement Factor

[7] As noted by *Edgar* [1976], whistler mode waves in the magnetosphere can undergo total internal reflections as they propagate from regions where the wave frequency (f) is above the lower hybrid frequency (f_{LHR}) to points where $f \simeq f_{LHR}$. This reflection process can occur numerous times, with the magnetosphere thus constituting a resonant ELF/VLF cavity wherein repeated reflections may lead to enhancement of wave energy. To properly quantify the manner in which wave energy is distributed within the magnetosphere, we must thus properly account for the fact that successive reflections may cause wave energy represented by a single injected ray to cross the same region numerous times before the wave power is significantly damped. To this end, we introduce the concept of the magnetospheric cavity enhancement factor (see below) to quantify the combined effects of magnetospheric reflections and Landau damping along the ray path. Landau damping, the primary damping mechanism for obliquely propagating whistler waves in the collisionless magnetospheric medium, is calculated using the formulation of *Brinca* [1981] and an electron distribution of $f(v) = 2 \times 10^5 v^{-4}$ cm^{-6}–s^3 as an approximate fit to recent energetic electron measurements [*Bell et al.*, 2002]. Figures 1a and 1b show two sample ray paths, as calculated using the Stanford VLF ray tracing code [*Inan and Bell*, 1977], and the associated Landau damping for each path. The ray path and attenuation change dramatically with the input parameters, as is examined in greater detail below.

[8] Spacecraft observations indicate that a single whistler mode wave can magnetospherically reflect up to at least 40 times before being significantly damped [*Smith and Angerami*, 1968; *Edgar*, 1976; *Gurnett and Inan*, 1988], resonantly interacting with, and pitch angle scattering, energetic electrons at all points along the ray path. We nevertheless focus our attention on the magnetic equator because the slow variation of the Earth's magnetic field at that point allows for the longest interaction time for wave-particle interactions and hence the highest diffusion (or scattering) coefficients. We then divide the magnetic equator into equally sized radial "bins" of, e.g., $0.1L$ in length and, for each equatorial crossing, note the location of the ray in L shell and assign it to the appropriate L bin. To arrive at the cavity enhancement factor for each L bin, we simply sum the normalized wave power (i.e., starting with a value of unity at the injection point) for every crossing of that bin by any ray.

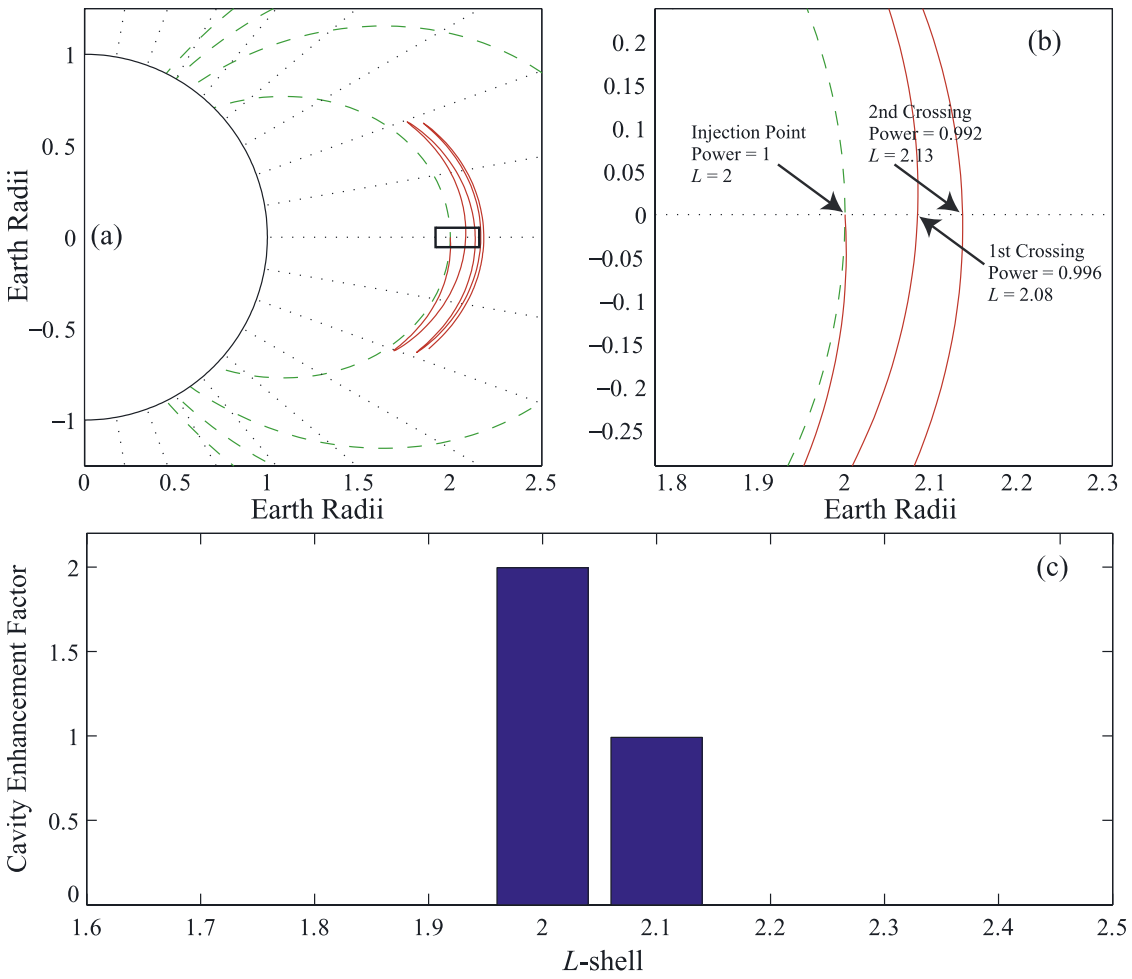

Figure 2. (a) Ray path of a 2.5 kHz signal injected at the geomagnetic equator at $L = 2$ with an initial wave normal angle of $-85°$. (b) An expanded portion from the ray path shown in Figure 2a showing the injection and the first two magnetic equatorial crossings. The normalized power, as calculated by Landau damping, and the L shell location of the ray are shown at each crossing. (c) The cavity enhancement factor after signal injection plus the first two equatorial crossings. At the first crossing, the ray is located at $L = 2.08$ and it has a normalized power of 0.996. If the L bins are $0.1L$ in length, then the $L = 2.0$ shell would be illuminated with a cavity enhancement factor of $1 + 0.996 = 1.996$. At the second crossing, the ray is located at $L = 2.13$ and has a normalized power of 0.992. Therefore the $L = 2.1$ shell would be illuminated with a cavity enhancement factor of 0.992.

[9] To illustrate this concept more clearly, consider the ray path, shown in Figure 2a, of a 2.5 kHz wave injected from $L = 2$ at the magnetic equator with an initial wave normal angle of $-85°$. For simplicity, only the injection and the first two equatorial crossings are expanded and shown in more detail in Figure 2b, along with the normalized wave power as attenuated by Landau damping and the location in L shell of the ray at each magnetic equatorial crossing. We then divide the magnetic equator into bins such that the ray position at injection ($L = 2.0$) and first equatorial crossing ($L = 2.08$) are both assigned to the $L = 2.0$ shell, and the ray position at the second equatorial crossing ($L = 2.13$) is assigned to the $L = 2.1$ shell. Finally, for each L bin, we sum the normalized wave power of the ray at every equatorial crossing within that bin to determine the resulting cavity enhancement factor. Referring again to Figure 2b, the cavity enhancement at the $L = 2.0$ shell is 1.996 (normalized power of 1.0 at injection plus a ray power of 0.996 at the first crossing) and 0.992 at the $L = 2.1$ shell. Of course, had we examined more than just the first two crossings, the cavity enhancement factor at both the $L = 2.0$ and the $L = 2.1$ regions may have been higher and the ray may also have propagated (and thus carried wave energy) to additional L shells. Figure 2c displays the cavity enhancement factor at the $L = 2.0$ and $L = 2.1$ shells after the first two equatorial crossings. It is important to note that a cavity enhancement factor greater than unity does not imply amplification of the wave power; it simply represents the fact that, for example, an injected signal of 1-s duration would cross the geomagnetic equator multiple times over a time period longer than 1-s, scattering electrons each time. A cavity enhancement factor of 1.5 would imply that this signal could be 1.5 times more effective in pitch angle scattering than it would have been in the absence of magnetospheric reflections. Alternatively, for the case of injection of a continuous wave train, we can think of the enhancement factor as the factor by

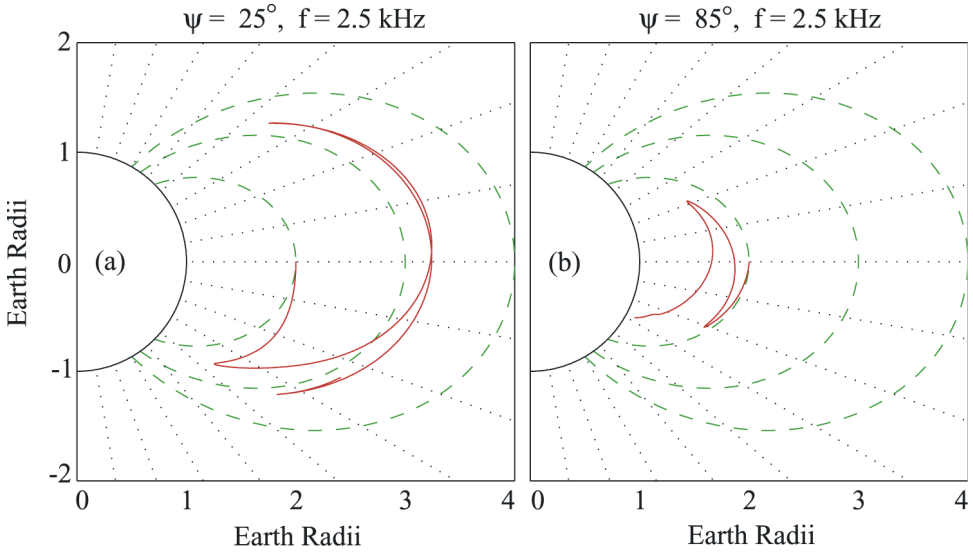

Figure 3. (a) Ray path of a wave injected at $L = 2$ at the geomagnetic equator, at an initial wave normal angle of 25°. The ray path traverses a very large region of the magnetosphere within the first few magnetospheric reflections. Rays with an initial outward pointing wave normal angle, as seen in Figure 2, tend to move very quickly to their settling L shell. (b) A ray with an initial wave normal angle of 75° is absorbed in the ionosphere very quickly.

which the total wave power multiplicatively increases with time as the wave energy is stored within the cavity. The magnetospheric reflections thus allow a single wave packet to interact with the energetic particles multiple times, with the wave power density decreasing with time. Accordingly, with several equatorial passes, the cumulative normalized power at a given L shell region is greater than unity.

[10] We also note that the cavity enhancement factor discussed herein differs from the cavity enhancement "gain" factor, G_c, described by *Inan et al.* [2003]. The latter was determined by weighting each equatorial crossing (regardless of the L value) with the wave power density at that point. The convention adopted in the present paper quantifies more precisely the L shell distribution of the wave energy, accounting for the fact that successive rays can cross different L bins. The two approaches are similar in that we can arrive at G_c by simply summing the cavity enhancement factor at the different L bins.

3. Simulation Results

[11] Our objective as discussed above is to quantify the projection of electromagnetic wave power onto a specific L shell region from a particular injection point in space. At any given time, it may be desirable to project wave power either to regions close to the satellite location or to L shells far away from the source. The input parameters (wave frequency and wave normal angle at injection) are likely to be different depending on the location of the satellite and the region where we wish to project wave power. We therefore simulate a substantial number of rays with a range of input parameters so that conclusions can be drawn with regards to appropriate frequencies and wave normal angles. One particular question of practical interest is to to determine the number and location of in situ sources needed to completely illuminate the region $1.3 < L < 3.5$ with ELF/VLF whistler mode wave energy.

[12] The simulation procedure we use is as follows: We first start with a given injection L shell and magnetic latitude. We consider three such L shell locations, $L = 1.5$, $L = 2.0$, and $L = 2.5$, as well as two geomagnetic latitudes, the equator and a latitude of 20° along each field line. This set of parameters constitutes a total of six different injection source sites. For each source site, we then inject waves at 100 different frequencies ranging from 1 to 10 kHz, in increments of 0.1 kHz, and, for each wave frequency, with initial wave normal angles from $-75°$ up to the resonance cone if $f > f_{LHR}$ or up to $-89.9°$ for $f < f_{LHR}$, with each wave normal angle separated by 0.1°. For each ray, we also calculate the path-integrated Landau damping and the cavity enhancement factor at the geomagnetic equator. The frequency range is chosen to encompass frequencies ranging from well below the local LHR frequency at all equatorial regions in the inner radiation belts up to a frequency for which magnetospheric reflections no longer occur. We consider initial wave normal angles that are pointing away from the Earth, $\psi < 0$, because rays with an initial inward pointing wave normal angle, $\psi > 0$, tend to take a longer time to reach their settling L shell (see below) or get absorbed into the ionosphere. Figure 3 shows the ray paths for two 2.5 kHz rays, one with an initial wave normal angle of 25° and the other 85°.

[13] The bulk of the simulation results shown are for a source located at $L = 2$ for which we separately examine equatorial and off-equatorial injections. However, before presenting the bulk of the simulation results, it is instructive to briefly explore whistler mode wave behavior in the inhomogeneous magnetospheric medium, especially the phenomena of the wave energy settling on a prescribed L shell (dependent only on wave frequency) and also the relationship between initial wave parameters (frequency,

wave normal angle) and the lifetime (i.e., cavity enhancement factors).

3.1. *L* Shell Settling and Wave Lifetimes

[14] Whistler mode waves propagating in the magnetosphere have the strong tendency, within the course of few initial magnetospheric reflections, to settle on an L shell where the wave frequency is approximately equal to the equatorial f_{LHR} [*Thorne and Horne*, 1994; *Ristic'-Djurovic' et al.*, 1998]. Manipulation of the wave frequency thus represents a first order means for controlling the illumination of a particular L shell. The LHR frequency ($f_{LHR} \sim (f_{He}f_{Hi})^{1/2}$ for $L = 2$, where f_{He} is the electron gyrofrequency and f_{Hi} is the ion gyrofrequency), is generally larger at locations closer to the Earth's surface. To selectively target lower L shell field lines, frequencies higher than the local LHR should be used, while lower frequencies should be used to project power toward higher L shells. This behavior is a strong function of wave frequency and does not change substantially with the injection location (L shell and geomagnetic latitude) or injection wave normal angle, although some exceptions will be noted. However, waves with an initially smaller normal angle or waves injected off the magnetic equator tend to propagate farther from their injection point before returning back, thereby taking a longer time to reach their settling L shell. Figure 4a demonstrates this principle by showing L shell location versus group travel time for four separate injections from $L = 2$ ($f_{LHR} \sim 2.5$ kHz) of 4 kHz waves; all four rays move, as expected, to lower L- shells and eventually settle on $L \sim 1.72$, where the equatorial f_{LHR} is ~4 kHz.

[15] The presence of path-integrated Landau damping greatly limits the ability of a whistler mode wave of a given frequency to reach its settling L shell without significant power loss. For in situ injections, waves injected above the local f_{LHR} or off the geomagnetic equator experience especially strong damping [*Bortnik et al.*, 2003a]. To clarify the preceding point, Figure 4b shows that Landau damping for the kind of rays discussed above result in all four rays to be damped by 10 dB after only 10 s so that these rays do not do not reach their settling L shell with significant intensity. Nonetheless, inspection of Figure 4a indicates that the rays have begun propagating toward lower L shells at this point, with two out of the four rays reaching $L \sim 1.8$. The various tradeoffs apparent from the above discussion, between injecting higher or lower frequency waves at equatorial and off-equatorial sites, are examined in more detail below.

3.2. Injections at the Geomagnetic Equator

[16] We first consider a single wave-injection source at $L = 2$ at the magnetic equator radiating 2.5 kHz waves, just below the local lower hybrid resonance frequency (~2.55 kHz). Such waves tend to propagate slightly outward and are damped more slowly than waves with frequencies higher than the local f_{LHR} [*Bortnik et al.*, 2003a]. The resultant ray path and damping are also dependent on the wave normal angle at injection, with wave normals initially closer to the resonance cone persisting much longer and resulting in larger cavity enhancement factors. This point is illustrated in Figure 5, which shows that for 2.5 kHz waves, changing the wave normal at injection injection (ψ) from $-75°$ to $-85°$ to $-89°$ results in progressively longer ray lifetimes and larger cavity enhancement factors. However, the rays injected with $\psi = -75°$ and $-85°$ disperse much farther than the ray injected $\psi = -89°$ and hence can interact with energetic electrons over a broader range of L shells. Examining rays injected at a continuum of normal angles from $-75°$ to $-89.9°$ indicates that, although 2.5 kHz waves usually propagate slightly outward from $L = 2$, certain L shells can be preferentially targeted by carefully choosing the injection wave normal angle. For example, as shown in Figure 6, a 2.5 kHz wave injected from the equator at $L = 2$ with $\psi = -80°$ remains in the $L = 2.2$ equatorial region during most of its lifetime but also crosses the magnetic equator near $L = 2.2$, $L = 2.1$ and $L = 2.0$. Conversely, a 2.5 kHz wave initially with $\psi = -89°$ remains very close to the injection source and does not significantly illuminate remote L shells.

[17] For comparison purposes, we also show the effect of injecting, from $L = 2$ at the geomagnetic equator, waves with frequencies both well below and above the local f_{LHR} of 2.55 kHz. As stated earlier, waves at a frequency below (above) the local f_{LHR} generally move to higher (lower) L shells and are also damped more slowly (quickly). As a consequence of longer lifetimes, lower-frequency waves also tend to attain overall larger cavity enhancement factors, although the L shell regions of wave energy deposition differs from that of higher-frequency waves. Figure 7 demonstrates these effects by showing the result of injection, again from $L = 2$ at the equator, of both a 1 kHz wave with $\psi = -85°$ and a 4 kHz wave with $\psi = -85°$. The 1 kHz wave immediately propagates to higher L shells and persists for well over 60 s, whereas the 4 kHz wave moves closer to the Earth and its normalized power is reduced by ~10 dB within 10 s. Additionally, the maximum equatorial cavity enhancement factor for the 1 kHz ray occurs at $L \sim 2.8$ but occurs at $L \sim 2.0$ for the 4 kHz ray. Although the ray path in Figure 7 for the 4 kHz wave migrates down to $L \sim 1.7$, strong Landau damping prevents significant wave power from reaching those lower L shells.

[18] Our results indicate that it may be particularly difficult to project wave power to some regions of the magnetosphere with a single source located at $L = 2$. Attempting to direct wave energy to $L = 1.3$, for example, would require the use of higher-frequency (~9 kHz) waves that often tend not to undergo magnetospheric reflections and that also would Landau damped very quickly. On the other hand, taking advantage of cavity enhancement at L shells as far away as $L = 3.5$ is not possible with a single equatorial source at $L = 2$ even when 1 kHz waves are used (see top row of Figure 8). To fill larger regions of the plasmasphere with whistler mode wave energy, one must therefore vary the radial distance where the satellite is placed. For injections from locations closer to the Earth we expect that the higher f_{LHR} implies higher frequencies should be used to target the source L shell while lower frequencies should be used for injection sites farther from the Earth. As described previously, we examine the wave power propagation from in situ sources located at $L = 1.5$ and $L = 2.5$ and, to compare with the results shown earlier for a satellite located at $L = 2$, for 1 kHz, 2.5 kHz, and 4 kHz waves.

[19] While at $L = 2$ these three frequencies are below, approximately equal to, and above the f_{LHR}, respectively, at

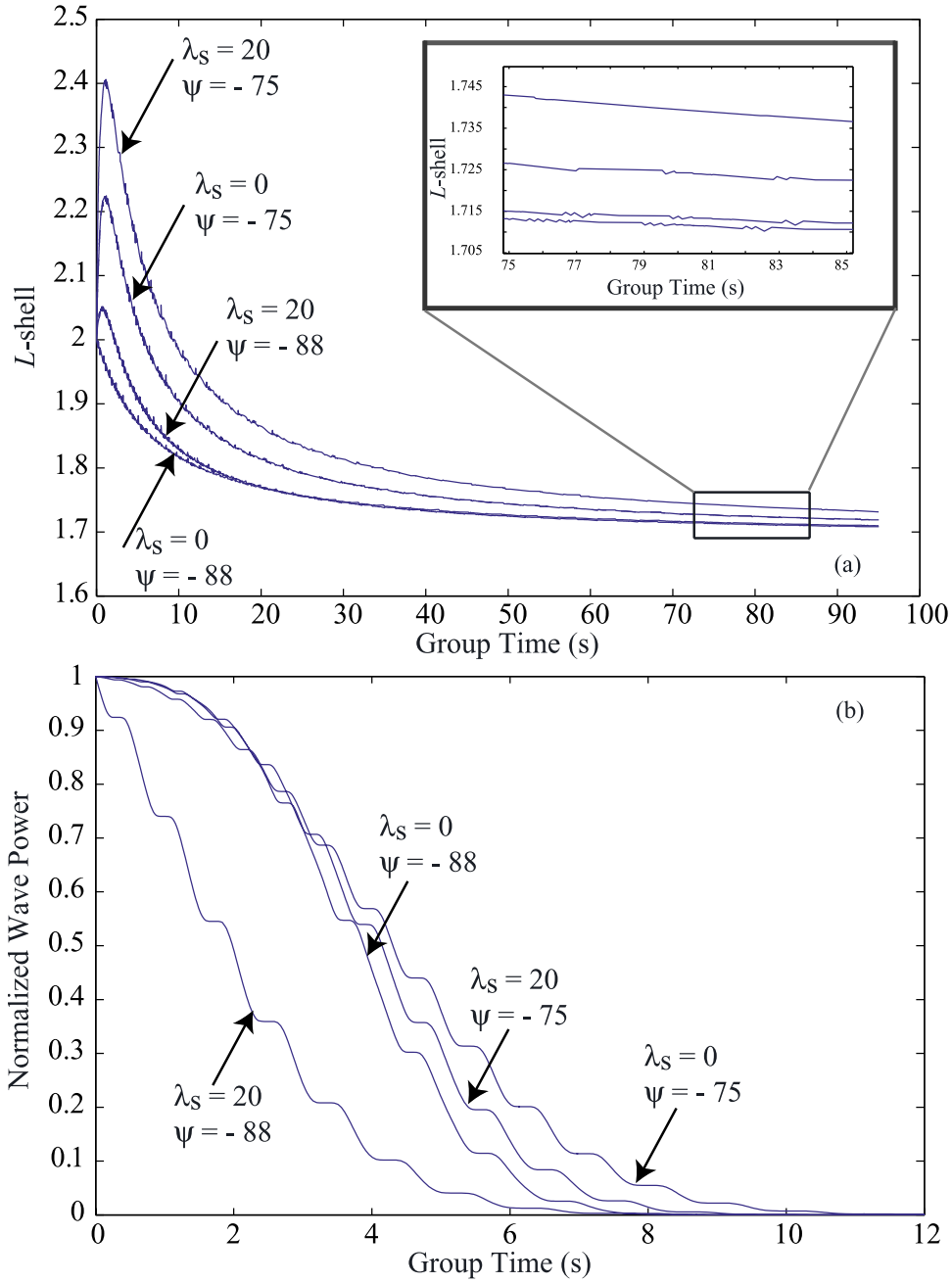

Figure 4. (a) L shell versus group time for four 4 kHz waves injected at $L = 2$. For a wide range of injection latitudes and wave normal angles, all 4 rays eventually settle on $L \sim 1.72$ (expanded portion shown in inset). Rays with a wave normal angle initially close to the resonance cone proceed to the settling L shell directly, as opposed to rays that are injected at $-75°$, which first propagate to higher L shells. (b) Path-integrated Landau damping for the four rays shown in Figure 4a. All four rays are damped within 10 dB within 10 s.

$L = 1.5$ all three frequencies are well below the local f_{LHR} (~6 kHz). Accordingly, injections from $L = 1.5$ at these wave frequencies propagate to higher L shells and exhibit very high cavity enhancement factors as a result of longer lifetimes. This result can be seen in Figure 9, showing a comparison of the integrated cavity enhancement factor (integrated along the ray path, then normalized, over all wave normal angles considered), for 1 kHz, 2.5 kHz, and 4 kHz waves, for injections from the equator at $L = 1.5$, $L = 2.0$, and $L = 2.5$. The top two rows of Figure 9 show injections from $L = 1.5$ and $L = 2.0$, with the 2.5 kHz waves injected from $L = 1.5$ having an integrated cavity enhancement factor at $L = 2$ that is a factor of ~4 higher than 2.5 kHz waves injected from $L = 2$. This result underscores the fact that wave frequencies below the local f_{LHR}, such as 2.5 kHz waves at $L = 1.5$, persist for longer times than waves above the f_{LHR}. Also note that since the equatorial f_{LHR} is ~6 kHz, all three frequencies shown exhibit cavity enhancement

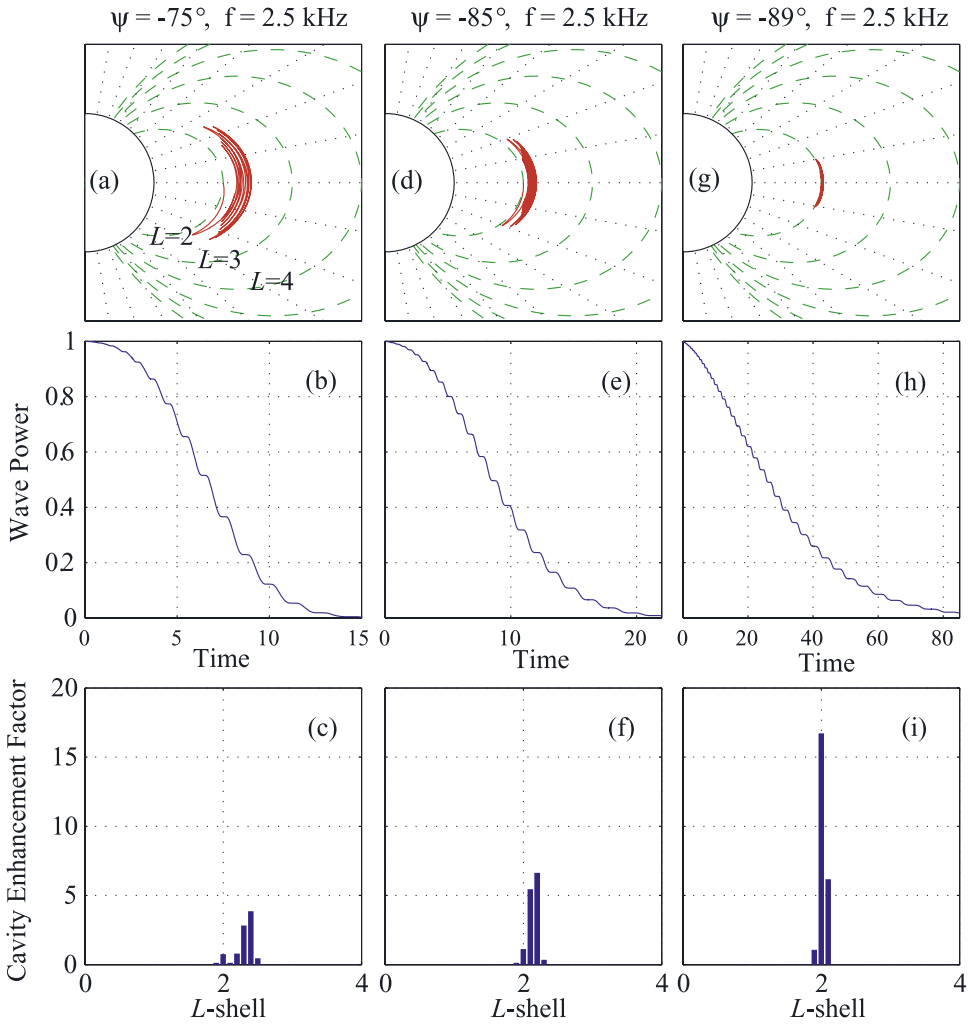

Figure 5. (a) Ray path of a 2.5 kHz (∼local f_{LHR}) signal injected at the equator at $L = 2$ at a wave normal angle of −75°. The wave propagates to L shells higher than the injection location. (b) Normalized wave power along the ray path. (c) Cavity enhancement factor at equator as a function of L-shell. (d) Ray path for a wave injected at a wave normal angle of −85°. (e) Wave energy persists for a longer time when the injection wave normal increases. (f) Cavity enhancement also increases when the injection wave normal angle increases. (g) An almost perpendicular injection wave normal angle almost results in numerous magnetospheric reflections near the $L = 2$ shell. (h) This signal persists for many tens of seconds. (i) The cavity enhancement factor is even larger with an injection wave normal angle of −89°.

primarily at L shells higher than $L = 1.5$. On the other hand, for 5 kHz, 6 kHz, and 7 kHz waves, corresponding to just below, approximately equal to, and above the local f_{LHR}, Figure 10 shows that the $L = 1.5$ region can be more effectively illuminated by simply changing the input wave frequency. It is interesting to observe that even at a frequency of 7 kHz, field lines for $L < 1.3$ are not illuminated because of very rapid Landau damping and fewer magnetospheric reflections. Taking advantage of cavity enhancement at locations extremely close to the Earth's surface ($1.1 < L < 1.3$) may therefore require sources placed at those L shells.

[20] In order to explore wave propagation from $L = 2.5$ (equatorial $f_{LHR} \sim 1.3$ kHz), we refer to the bottom row in Figure 9, which displays the integrated cavity enhancement factor at $1 < L < 4$ for 1 kHz, 2.5 kHz, and 4 kHz waves. As opposed to the previous source locations, 2.5 kHz and 4 kHz waves injected from $L = 2.5$ are above the local f_{LHR}; they therefore propagate down to lower L shells and get damped more quickly than similar frequency waves injected from $L = 1.5$ and $L = 2.0$. Interestingly, even though 1 kHz is below the f_{LHR} at all three source sites considered, injections from $L = 2.5$ still cause substantially lower integrated cavity enhancement factors. Clearly, waves which are 5 kHz below the local f_{LHR}, as is a 1 kHz wave injected from $L = 1.5$, endures much longer than a wave frequency much closer to the local f_{LHR}. In fact, among the three source locations investigated so far, the integrated cavity enhancement factor is smallest for injections from $L = 2.5$. Despite the smaller cavity enhancement, the results demonstrate that for the sample frequencies shown, a single source at the geomagnetic equator at $L = 2.5$ can effectively illuminate at L shells from $L \sim 2.1$ up to $L \sim 3.2$. This illumination range does not increase significantly with the

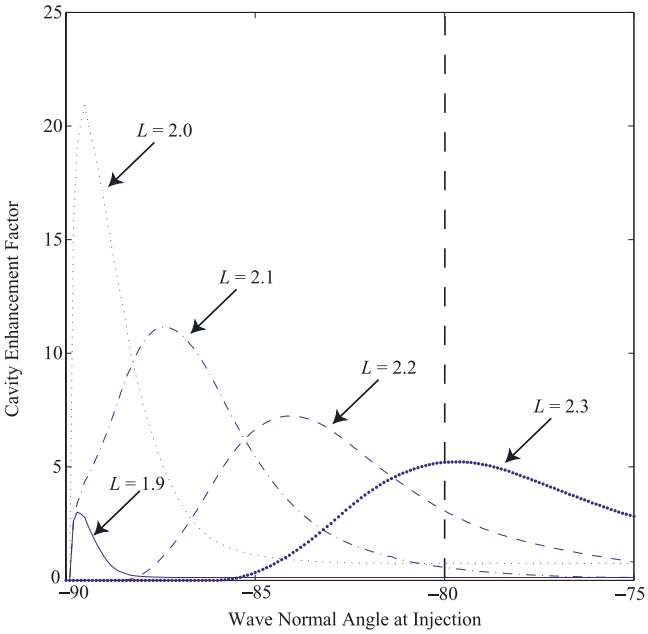

Figure 6. Cavity enhancement factor at L = 1.9, 2.0, 2.1, 2.2 and 2.3 as a function of injection wave normal angle for a 2.5 kHz wave at L = 2 at the geomagnetic equator. A vertical line drawn from the horizontal axis represents how wave power disperses in L shell for a single injection at a specific initial wave normal angle. For example, for $\psi = -80°$ (dashed vertical line), a 2.5 kHz ray injected at L = 2 at the equator will propagate out to slightly higher L shells, resulting in a cavity enhancement factor of ~5 at L = 2.3 and ~4 at L = 2.2.

inclusion of additional, higher frequencies because these frequencies would be damped before reaching their settling L shell.

3.3. Off-Equatorial Injections

[21] Up to this point we have considered wave injection from sources located solely at the geomagnetic equator. In practice, any spacecraft-based source in orbit would necessarily spend a lot of time at locations off the equator; it is thus useful to consider the injection of waves from such a source at other locations. *Bortnik et al.* [2003a, 2003b] has examined in considerable detail the disparity in ray lifetimes, and by implication cavity enhancement factors, for off-equatorial versus equatorial injections.

[22] For the simulations considered here, insight into the differences between equatorial and off-equatorial injections can be gained by comparing the results in Figure 11 with the results shown in Figure 5 earlier. Here, we inject three 2.5 kHz rays from L = 2 at a geomagnetic latitude of 20°, with initial wave normal angles of −75°, −85°, and −89°, respectively. For each case, the off-equatorial injection leads to more rapid damping of the wave and illumination of a wider range of L shells than the corresponding equatorial injection.

[23] Referring back to Figure 8, we can more clearly see the differences between the two different source sites considered. The top row shows the integrated cavity enhancement factor for 1 kHz, 2.5 kHz, and 4 kHz waves injected from L = 2 at the geomagnetic equator. The off-equatorial injections, shown in the bottom row, consistently result in smaller integrated cavity enhancement factors but illuminate a broader range of L shells. For instance, 2.5 kHz waves injected at the equator from L = 2 project power up to L = 2.5 with a normalized integrated enhancement factor as high as ~6; injections from 20° can affect L shells as far as L = 2.7 but also result in lower cavity enhancement factors. While similar results can be also be demonstrated for injections from L = 1.5 and L = 2.5, they are not shown here for the sake of brevity.

[24] The tradeoff between greater, more localized cavity enhancement factors for equatorial injections versus smaller, more distributed cavity enhancement factors for off-equatorial injections may be important in the design of a practical system for controlled precipitation of radiation belt electrons.

3.4. Comparison and Analysis

[25] To assess the feasibility of whistler mode illumination, via in situ injection, of the plasmasphere, we have investigated the effects of varying three principal parameters: injection source location, wave frequency and initial wave normal angle. The results presented thus far allow us to highlight the primary tradeoffs in considering a combination of these parameters. First, it is important to observe that across all injection locations considered (L = 1.5, L = 2 and L = 2.5) there is a consistent pattern of equatorial injections resulting in a much larger integrated cavity enhancement factor than off-equatorial injections but also affecting a narrower region of L shells. Second, as discussed earlier, frequencies below (above) the local f_{LHR} have longer (shorter) lifetimes with larger (smaller) resultant cavity enhancement factors and propagate to higher (lower) L shells. Finally, rays with an initial wave normal angle that is nearly perpendicular to the ambient magnetic field have much longer lifetimes and stay closer to the source location than less oblique initial wave normal angles. To maximally target the source L shell, the optimum condition would be to use a source, situated at the equator of the desired L shell, injecting waves at a frequency equal to the local f_{LHR} at wave normals very close to the resonance cone. Rays with an initial wave normal closer to parallel to the magnetic field, on the other hand, would disperse to more distant locations over a broader region of L shells, albeit with a shorter lifetime and smaller resultant cavity enhancement factors.

[26] We can quantify the role of the initial wave normal and frequency by studying the dispersal of wave power from a single L shell for a wide range of input parameters. For example, consider two sources at L = 2, one at the equator and another at a geomagnetic latitude of 20° on the same field line. Given these two locations, we set out to identify the frequencies and injection wave normal angles that lead to maximum cavity enhancement factors in a given L shell range, $1.8 < L < 2.2$. On the basis of the above discussion, we expect that for a source at L = 2, the L = 2.0 shell is best targeted with 2.5 kHz waves injected with initial wave normal angles close to the resonance cone. On the other hand, the L = 1.8 shell would best be targeted with waves ~4 kHz and the L = 2.2 shell with ~2 kHz waves. Figure 12 shows the equatorial cavity enhancement factor at

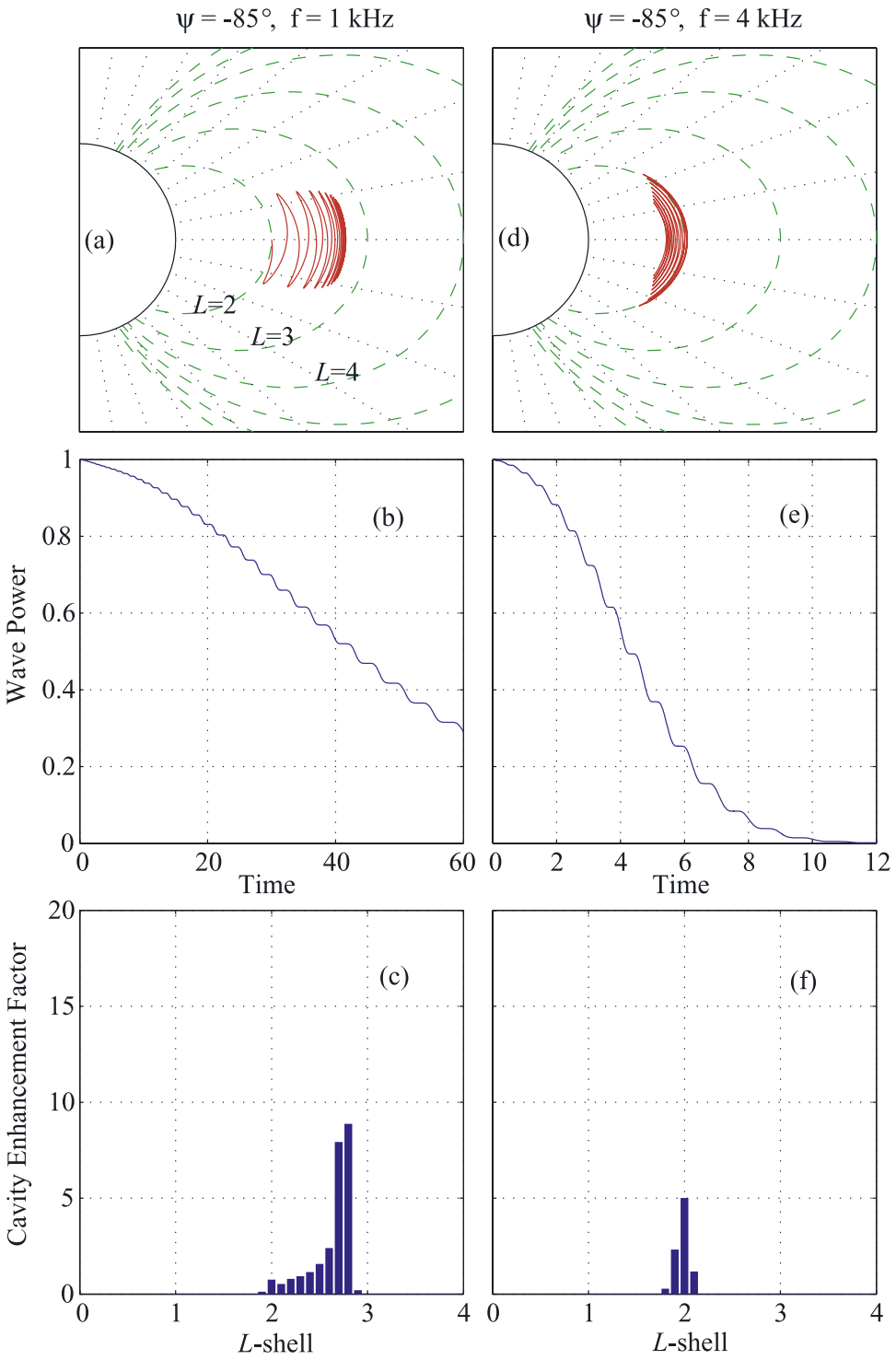

Figure 7. (a)–(c) Ray path, Landau damping and cavity enhancement factor for a 1 kHz signal injected at $L = 2$ at the equator at a wave normal angle of −85°. A wave well below the local f_{LHR} (~2.5 kHz) persists for well over 60 s. (d)–(f) A 4 kHz signal injected at a similar location propagates to lower L shells and damps much more quickly than the 1 kHz signal. Also, the cavity enhancement is smaller and occurs at lower L shells.

L = 1.8, 1.9, 2.0, 2.1, 2.2 as a function of wave frequency and initial normal angle for waves injected from $L = 2$ at the equator and at a geomagnetic latitude of 20°. The left (right) column represents the results of equatorial (off-equatorial) injections; corresponding pixels in the 5 individual panels for each L shell range corresponding to a single injection point. As an example, consider a 5 kHz ray injected at $L = 2$ at the equator at a wave normal of −85° (the corresponding point is highlighted with asterisks on the left column in Figure 12). This wave primarily moves inward and with

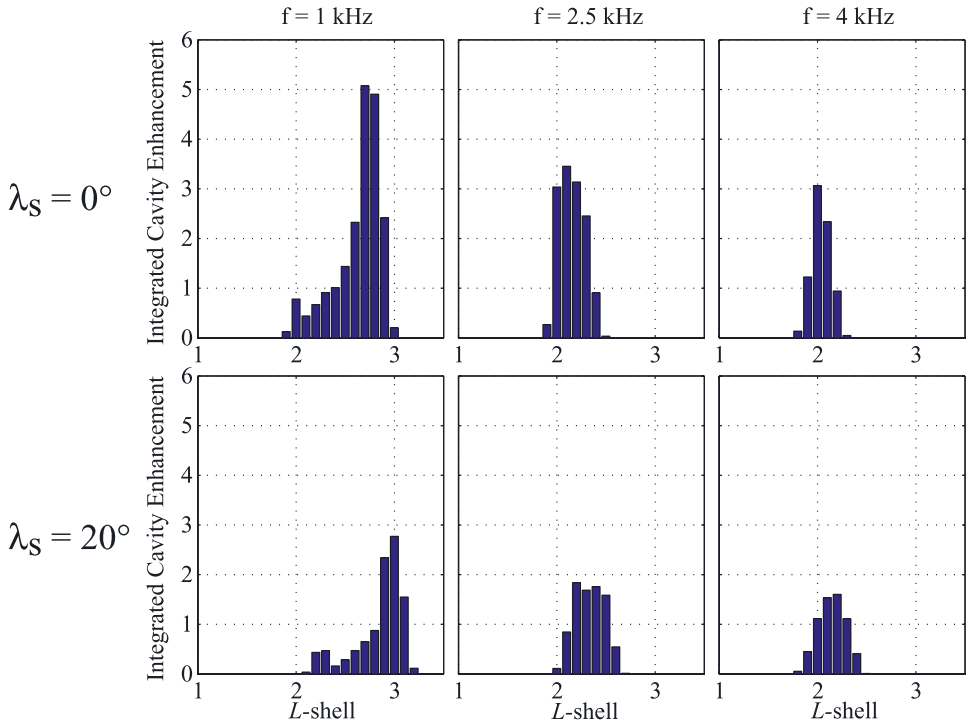

Figure 8. Cavity enhancement factor integrated over all wave normal angles considered, $-75°$ to $-89.9°$ if $f < f_{LHR}$ or $-75°$ to θ_{res} if $f > f_{LHR}$. Result is normalized by the total number of injections. The cavity enhancement is shown at L-shells from $1 < L < 3.5$ for 1 kHz, 2.5 kHz and 4 kHz waves injected from $L = 2$; with equatorial injections shown across the top row and off-equatorial across the bottom row. For each frequency, equatorial injections have a much larger integrated cavity enhancement factor but also illuminates a smaller range of L shells.

resultant cavity enhancement at lower L shells. Thus the $L = 2.2$ shell is not significantly illuminated if a wave with these input parameters is injected from the geomagnetic equator at $L = 2$. The injection of the same wave from a geomagnetic latitude of 20°, however, does result in minimal cavity enhancement at $L = 2.2$. For clarity, the ray path and cavity enhancement factor for this individual injection parameters are illustrated in Figure 12.

[27] As expected, the cavity enhancement factor at lower L shells are smaller than those at higher L shells. The fundamental reason for this difference lies in the fact that the higher frequency waves which tend to move inward are also the waves that will be damped the strongest [*Bortnik et al.*, 2003a]. Additionally, the appearance of a resonance cone in the refractive index surface at frequencies above the local f_{LHR} narrows the region in wave normal space available for propagating waves. The resonance cone can be seen as the sloping region of white in the lower right hand corner of each panel in Figure 12. As the frequency increases, propagating wave solutions are possible over an increasingly narrow range of wave normal angles. The resonance cone becomes a factor at higher frequencies for off equatorial injections (right column) since the local LHR frequency is higher at points off the equator. As such, a 4 kHz wave injected from $L = 2$ at the equator is above the local f_{LHR} whereas a similar frequency wave would be below the local f_{LHR} at a latitude of 20°. These facts slightly modify the appropriate frequencies and wave normal angles needed to illuminate target L shells. Referring to the middle panel in the first and second column of Figure 12, it can be seen that, for a source located at $L = 2$ targeting power on $L = 2$, one would use ~2.5 kHz waves for injections at the equator whereas ~3 kHz waves should be used for injections at a latitude of 20°. The final point we should highlight here is that, although the resolution may not be high enough to clearly discern the difference, off-equatorial injections (displayed in the right column of Figure 12) indeed result in lower cavity enhancement factors than equatorial injections. On the other hand, if we had displayed additional L shells, we would see that these rays also propagate over a wider range of L shells than similar rays injected at the equator. This tradeoff, higher cavity enhancement factors versus broader projection of power, can be leveraged effectively in designing a practical system aimed at controlled precipitation of energetic radiation belt electrons. [*Inan et al.*, 2003].

4. Effects of Antenna Radiation

[28] Our discussions thus far indicate that whistler mode wave energy injected in situ from a given position can be efficiently (i.e., with relatively large cavity enhancement factors) directed to a L shell region as far away as $\sim 0.3L$ from the source for locations closer to the Earth and up to $\sim 1L$ for locations farther from the earth. In formulating these results, we did not consider the restrictions that would inevitably be present as a result of the dramatically different radiation properties of practical antennas immersed in a

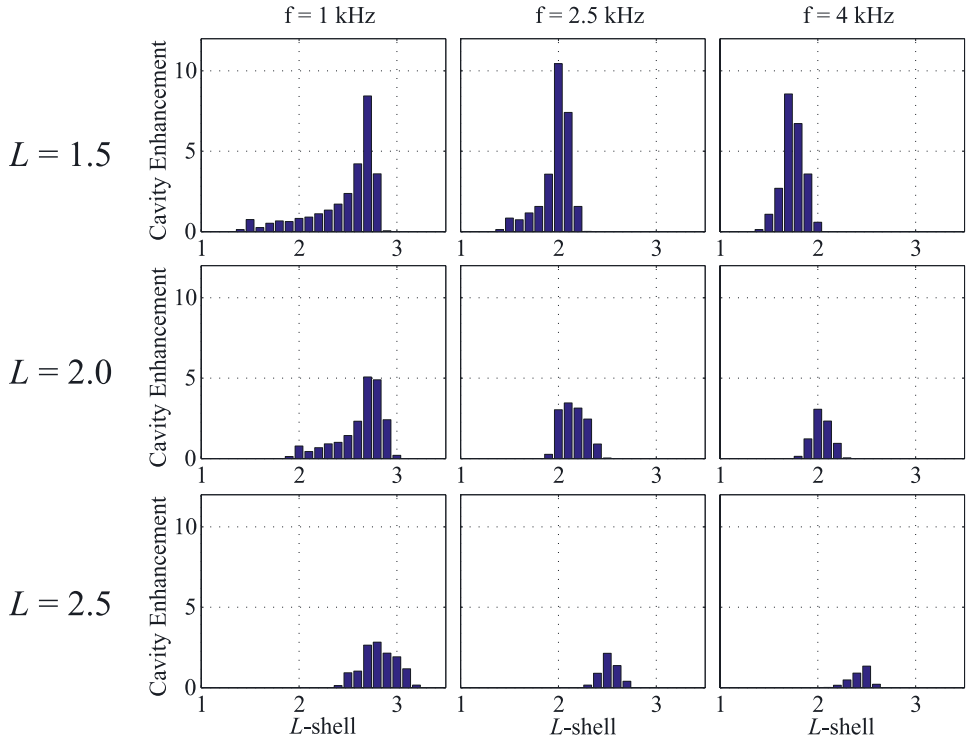

Figure 9. This figure, similar to Figure 8, shows the cavity enhancement factor integrated over all wave normal angles considered and then normalized by the total number of injections. The three columns display the three sample wave frequencies of 1 kHz, 2.5 kHz, and 4 kHz; and each row represents the three separate injection source sites (L = 1.5, 2.0, and 2.5). All waves were injected from the magnetic equator. As the injection location moves farther from the Earth, the normalized cavity enhancement decreases for each frequency shown.

magnetosplasma. We now investigate the effects of practical antenna efficiency and radiation pattern on our results using the model presented by *Wang and Bell* [1970] of a short electric dipole transmitting antenna immersed in a cold, magnetized plasma. In adapting the *Wang and Bell* [1970] model to our results, we note that they ignored the complicating effects of the plasma sheath as well as any nonlinearities that may arise with the inclusion of warm plasma effects. Although as yet there exists no universally accepted model of the behavior of a space-based antenna, we note that our results can also be used with any other previously developed or future antenna-in-magnetoplasma-model. We choose the *Wang and Bell* [1970] for our work because it specifically addressed the VLF frequency range that we are interested in and presents results that encompass the magnetoplasma parameter ranges of interest.

[29] The *Wang and Bell* [1970] model establishes two primary constraints on whistler mode radiation with dipole

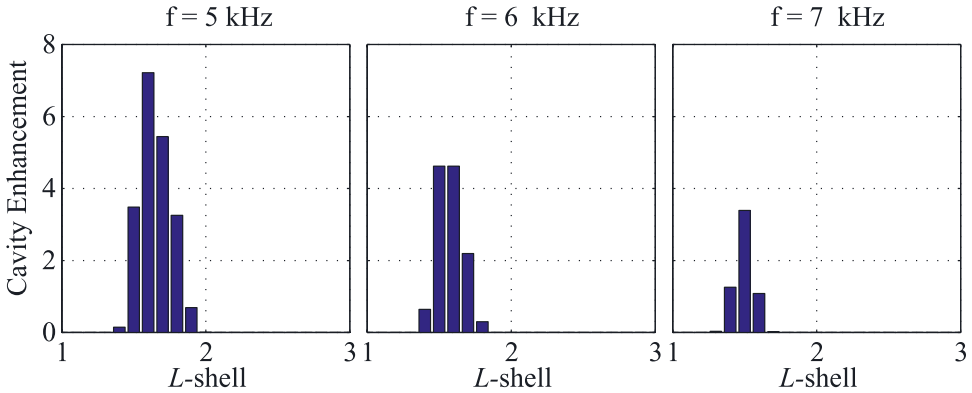

Figure 10. Integrated cavity enhancement factor for injection from the geomagnetic equator at L = 1.5, where the equatorial f_{LHR} is approximately 6 kHz. The three sample wave frequencies are therefore more appropriate for targeting the source site, as opposed to 1 kHz, 2.5 kHz, or 4 kHz waves shown earlier (see top row of Figure 9).

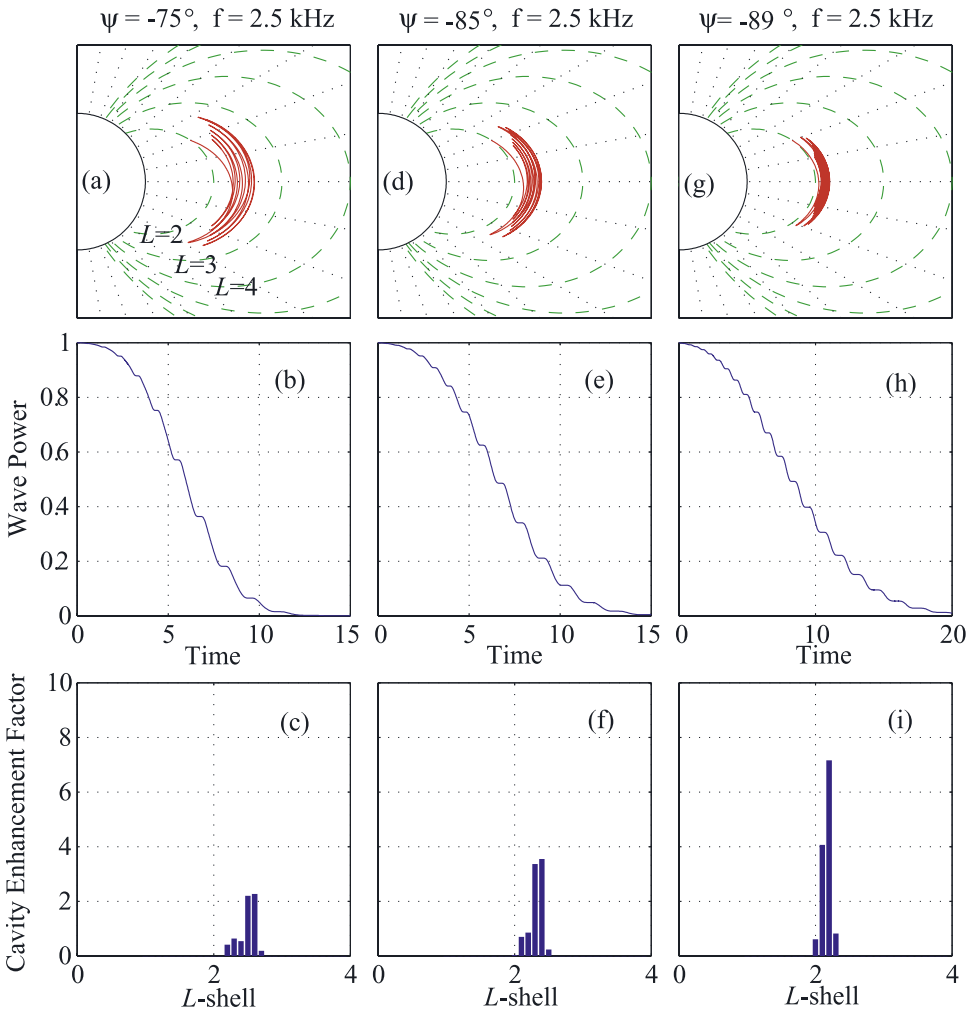

Figure 11. (a) Ray path of a 2.5 kHz (∼local equatorial f_{LHR}) signal injected at $L = 2$ at $\lambda = 20°$ at a wave normal angle of $-75°$. Note that the wave energy propagates out to higher L-shells as compared to Figure 5a. (b), (c) Normalized wave power along ray path and cavity enhancement factor as a function of L shell. (d) Ray path for a wave injected at a wave normal angle of $-85°$. (e), (f) Wave energy persists for a longer time and the cavity enhancement factor increases when the injection wave normal increases. (g) A 2.5 kHz wave injected at a $\lambda = 20°$ at $L = 2$ stays closer to the $L = 2$ shell if initial wave normal angle is almost perpendicular to the Earth's magnetic field. The ray still propagates out much farther than the corresponding equatorial injection shown in Figure 5g. (h), (i) Landau damping and cavity enhancement factor for the ray path shown in Figure 11g.

antennas in the magnetosphere. First, a short, electric dipole has negligible radiation resistance if the driving frequency is more than ∼10% below the local f_{LHR}. Hence a source located at the equator at $L = 2$ would not effectively radiate VLF waves below ∼2.3 kHz, which clearly indicates that our results presented above for 1 kHz waves should be properly qualified. Secondly, a VLF dipole antenna in a magnetoplasma emits the primary portion of its total radiated power as waves whose wavelength is approximately equal to the antenna length. This conclusion can be inferred from equation (8) in the work of *Wang and Bell* [1970], where the radiation resistance for antennas perpendicular to the magnetic field is negligible unless the argument in the $\frac{\sin^4(\lambda n_x)}{(\lambda n_x)^4}$ term is ∼1 (notation defined by *Wang and Bell* [1970]). λn_x is approximately 1 if the wavelength is on the order of the antenna length. In an anisotropic medium such as in the Earth's inner magnetosphere, wavelength is dependent on both wave frequency and direction with respect to the ambient magnetic field. For a given location and wave frequency, the wavelength is uniquely determined by the wave normal angle. For antenna lengths of ∼200–500 m and for the few kHz waves considered here, waves must have a wave normal angle within a few degrees of the resonance cone (or within a few degrees of $\psi = 90°$ if $f < f_{LHR}$) in order to satisfy the requirement for the radiated wavelength to be approximately equal to the antenna length.

[30] These above restrictions limit the allowable wave frequencies and the range of wave normal angles that can be used to direct the dispersal of whistler mode wave energy. While in Figures 8, 9, and 10, we integrated and normalized over wave normal angles up to $-75°$, the *Wang and Bell* [1970] theory suggests that there would be negligible

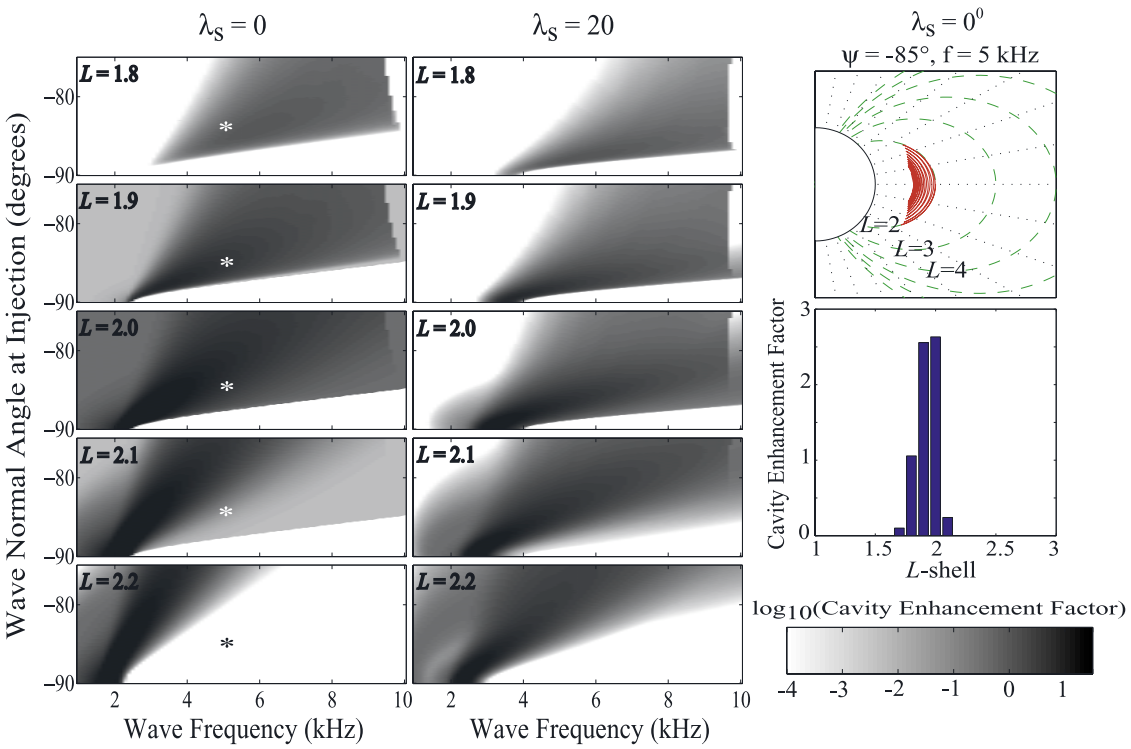

Figure 12. The first two columns display the cavity enhancement factor at $1.8 < L < 2.2$ for waves injected at $L = 2$ with the injection latitude shown at the top of each column. Within each column, corresponding positions in each panel represent a single injection. The asterisk in each panel in the left column represents the cavity enhancement caused by a 5 kHz wave injected at the equator at a wave normal angle of $-85°$. Note that the wave does not cross the equator near $L = 2.2$ and primarily moves inward. For clarity, the ray path and cavity enhancement factor for this injection is shown on the right along with the common color bar.

radiated power beyond $\sim\pm85°$. We thus expect that antenna radiation considerations, which limit effective radiation to only the most oblique wave normal angles, would then limit the L-shell range of illumination. To be consistent with the *Wang and Bell* [1970] model, we adjust the lower integration bound to be no more than three degrees away from the maximum wave normal angle considered ($-89.9°$ if $f < f_{LHR}$ or θ_{res} if $f > f_{LHR}$). Furthermore, we choose wave frequencies that are no lower than 90% of the local f_{LHR}.

[31] This result of the inclusion of antenna radiation considerations is illustrated in Figure 13, which shows the effects of restriction of the wave normal angles and wave frequencies considered for rays injected from $L = 1.5$, $L = 2.0$, and $L = 2.5$ from both the geomagnetic equator and a latitude of 20° along the field line. For each graph in Figure 13, we show the corresponding cavity enhancement factor for frequencies $\sim$10% below, approximately equal to, and 1 kHz above the local f_{LHR}, with the frequencies chosen for each injection site given in Table 1. Additionally, for each wave frequency chosen, we have integrated and normalized over only the first three degrees in wave normal angle.

[32] There are several important features of the results shown in Figure 13. As expected, the initial wave normal angle limitations necessitated by the *Wang and Bell* [1970] model result in cavity enhancement over a smaller range of L shells as compared to Figure 9. For instance, 2.5 kHz waves injected equatorially from $L = 2$, shown in white in the top middle graph of Figure 13, lead to relatively large cavity enhancement factors in the range $1.9 < L < 2.2$, whereas including the full angular range (middle column, 2nd row in Figure 9) leads to large cavity enhancement factors up to $L \sim 2.4$. The requirement that the wave frequency be no smaller than $\sim$90% of the local f_{LHR} also prevents the use of wave frequencies (generally 2–3 kHz below the local f_{LHR}) that would be suitable to target regions far from the injection site. This restraint is most evident for injections from $L = 1.5$, as shown in the left column of Figure 13, where the f_{LHR} at the geomagnetic equator and at a latitude of 20° is 6 kHz and 10 kHz respectively. The top panel, comparable to Figure 10, shows that restricting the angular and frequency range results in cavity enhancement just in the immediate vicinity of the transmitter location. Waves radiated from $L = 1.5$ and a latitude of 20° (refer to the bottom panel in the left column) are at such a high frequency, 9, 10, and 11 kHz, that no magnetospheric reflections occur. Sources this close to the Earth's surface can therefore be used to affect energetic electrons only on the first equatorial pass of the ray path, after which the ray energy is absorbed within the ionosphere. Another noteworthy feature is that the normalized, integrated cavity enhancement factor is larger when we integrate over only the first three degrees in wave normal space. Again referring to 2.5 kHz waves injected equatorially from $L = 2$, we see that cavity enhancement factor at $L = 2$ is $\sim$3 when the full

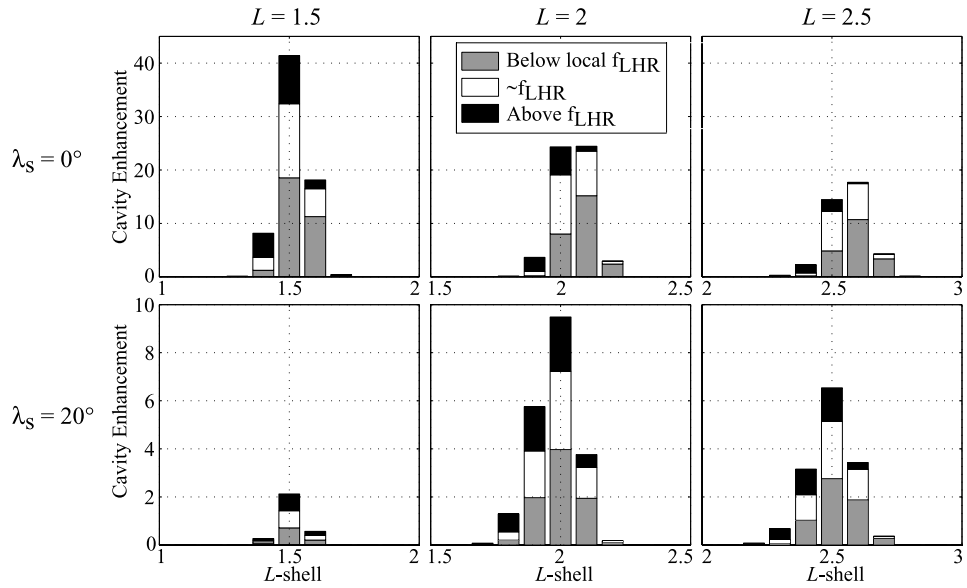

Figure 13. We show the effects of incorporating the frequency and angular limitations imposed by the use of short antennas in a magnetoplasma [*Wang and Bell*, 1970]. For each injection site, we select three wave frequencies, ~10% below, approximately equal to and 1 kHz above the local f_{LHR}. (Frequecies used given in Table 1.) For $f > f_{LHR}$, we inject rays with an initial wave normal angle from ψ_{res} to $\psi_{res} + 3°$. If $f < f_{LHR}$, we inject rays with an initial wave normal angle from $-89.9°$ to $-86.9°$. In all cases, we inject a total of thirty rays separated by 0.1° in wave normal angle. The contributing cavity enhancement factor for each frequency is given by the color code shown in the top, middle panel. Observe that wave frequencies below the local f_{LHR} result in the largest cavity enhancement factors.

angular range is considered (middle panel in Figure 9) and ~10 for the smaller range (shown in green in the top, middle panel in Figure 13). This result is a consequence of the fact that rays with an initial wave normal almost perpendicular to the ambient magnetic field have much longer lifetimes than those with lower initial wave normal angles. Hence integrating over a much broader range of wave normal angles does not add significantly to the cavity enhancement factor, and the small gain is then completely lost upon normalization over the number of injected rays. Thus even though the *Wang and Bell* [1970] model greatly reduces the allowable angular range for wave normals, the most persistent (i.e., the most efficiently stored) rays are still retained and available for illumination of particular L shell regions.

[33] For the six source sites studied here (L = 1.5, 2.0, 2.5 and λ_s = 0°, 20° for each L shell), a major overall conclusion is that only three sources, radiating power according to the *Wang and Bell* [1970] model, are required to project whistler mode wave energy from $1.4 \lesssim L \lesssim 2.7$. The affected L-shell region displayed in Figure 13 in fact represents a lower-bound because we only investigated a single off-equatorial location, λ_s = 20°. Simulating source locations at additional geomagnetic latitudes would necessarily increase the range of L shells upon which significant cavity enhancement factors can be attained.

5. Summary and Conclusion

[34] We have used the Stanford VLF ray tracing code [*Inan and Bell*, 1977] coupled with an accurate estimation of the path-integrated Landau damping, combined with the data set from *Bell et al.* [2002], to simulate a large number of whistler mode wave frequencies and injection wave normal angles at six different magnetospheric source locations. By introducing the magnetospheric cavity enhancement factor, we quantitatively account for the fact that an ELF/VLF wave represented by a given injected ray, because of repeated reflections, may resonantly interact with energetic electrons multiple times during multiple equatorial crossings before its energy is diminished. At each equatorial crossing, the wave power is placed into L "bins" and summation of the normalized power within each bin represents the cavity enhancement factor. Thus a cavity enhance-

Table 1. Wave Frequencies Simulated for the Six Different Injection Sites Shown in Figure 13[a]

	λ_s = 0°		λ_s = 20°	
	5.4 kHz		9 kHz	−89.4°
L = 1.5	6 kHz	−89.4°	10 kHz	−89.1°
	7 kHz	−88.9°	11 kHz	−88.8°
	2.3 kHz		3.8 kHz	
L = 2.0	2.5 kHz	−89.9°	4.2 kHz	−89.6°
	3.5 kHz	−88.7°	5.2 kHz	−88.9°
	1.2 kHz		2.0 kHz	
L = 2.5	1.3 kHz		2.2 kHz	−89.8°
	2.3 kHz	−88.1°	3.2 kHz	−88.5°

[a]At each location, the middle frequency is approximately equal to the local f_{LHR} while the top and bottom frequencies are ~10% below and 1 kHz above, respectively. Also shown are the resonance cone angles whenever they exist (i.e., whenever the frequency considered is above the local f_{LHR}). We calculate f_{LHR} using the relation $f_{LHR} \sim (f_{He} f_{Hi})^{1/2}$ where f_{He} is the electron gyrofrequency and f_{Hi} is the ion gyrofrequency. The strength of the Earth's magnetic field is calculated using a centered dipole model.

ment greater than unity does not suggest amplification of wave power; instead it simply reflects the fact that due to a number of magnetospheric reflections, the total integrated normalized power projected (over time) at a single L shell bin can be larger than unity.

[35] The initial analysis involved first specifying an injection location, L = 1.5, L = 2.0, L = 2.5 and a geomagnetic latitude of 0° and 20° for each L shell, and then investigating the behavior of injected rays at wave frequencies from 1 to 10 kHz by 0.1 kHz. For each wave frequency, we studied initial wave normal angles from −75° up to −90° (or the resonance cone if $f > f_{LHR}$). Examination of the results of these simulations has allowed us to assess the feasibility of projection of wave energy on particular L shell ranges in the inner radiation belts. In general, waves settle on L shells where the wave frequency is approximately equal to the lower hybrid resonance frequency at the geomagnetic equator on that L shell. Thus waves with frequencies below the local f_{LHR} move outwards from the injection site and wave frequencies above the f_{LHR} move inward. The injection wave normal angle further determines the behavior of the ray path, with rays having wave normal angles initially more perpendicular (parallel) staying closer to (dispersing farther from) the injection L shell.

[36] The inclusion of Landau damping in our results provides an accurate picture of where the largest cavity enhancement factors occur. Frequencies below the local f_{LHR} and waves with an initial perpendicular normal angle persist for a much longer time (up to ∼60 s in some cases) than waves with frequencies above f_{LHR}. Consequently, minimal cavity enhancement factors occur at L shells inward from the injection site because the high frequency waves that would be used to target those locations are also the waves that experience the strongest Landau damping. Additionally, for off-equatorial injections, while damping occurs more quickly than equatorial injections, resulting cavity enhancement factors can be significant over a broader range of L shells. These initial results indicate that before antenna radiation pattern is considered, only three sources are needed to illuminate the region of $1.3 \lesssim L \lesssim 3.5$ with relatively large cavity enhancement factors.

[37] We also investigated the effects that the use of a practical transmitting antenna in the magnetosphere would impose on our simulations, with the most applicable theory in this connection being the *Wang and Bell* [1970] model of a short, electric dipole radiating in a magnetized plasma. The two primary limitations imposed by this theory are constraints on the driving frequency and initial wave normal angle. According to the *Wang and Bell* [1970] theory, wave frequencies below ∼90% of the local f_{LHR} or initial wave normal angles beyond ∼3° of the resonance cone contain negligible radiated power. Thus for each source location, we repeated our analyses for a restricted range of wave frequencies and injection wave normal angles.

[38] In conclusion, our results indicate that even after incorporation of the limitations resulting from the *Wang and Bell* [1970] model, only three sources, in orbit and thus radiating alternately at both equatorial and off-equatorial sites at L = 1.5, L = 2.0 and L = 2.5 and utilizing driving frequencies no lower than ∼90% of the local f_{LHR}, are needed to illuminate (with significant cavity enhancement factors) the L shell range of $1.4 \lesssim L \lesssim 2.7$. Given that only two geomagnetic latitudes were studied, this L shell range, already comprising the bulk of the inner radiation belts, represents a lower limit to which we can project whistler mode wave energy. Additional minor changes to the results shown might come about with the inclusion of ray paths outside of the meridional plane, as would be possible with a three-dimensional ray tracer. With initial wave normals outside the meridional plane, there would be differences in the deposition of whistler mode wave energy, although we do not expect any substantial changes to our conclusions. *Cairó and Lefeuvre* [1986] have used three-dimensional ray tracing to study the propagation of ELF/VLF hiss in the magnetosphere. Their study indicates that highly oblique whistler waves (with initial wave normal angles in the range considered in this study) tend to see an azimuthal angle, ϕ, approximately constant in the course of their propagation.

[39] Finally, future investigations involve quantifying the precipitation signatures that would result from the in situ injection of whistler mode waves.

[40] **Acknowledgments.** The authors would like to thank Jacob Bortnik for his assistance. This research was supported by the Department of the Air Force under grant F19628-03-C-0059-P000003.

[41] Zuyin Pu thanks the reviewers for their assistance in evaluating this paper.

References

Abel, B., and R. M. Thorne (1998a), Electron scattering loss in the Earth's inner magnetosphere: 1. Dominant physical processes, *J. Geophys. Res.*, *103*, 2385. (Correction, *J. Geophys. Res., 104*, 4627, 1999.)

Abel, B., and R. M. Thorne (1998b), Electron scattering loss in the Earth's inner magnetosphere: 2. Sensitivity to model parameters, *J. Geophys. Res.*, *103*, 2397. (Correction, *J. Geophys. Res., 104*, 4627, 1999.)

Angerami, J. J., and J. O. Thomas (1964), Studies of planetary atmospheres: 1. The distribution of electrons and ions in the Earth's exosphere, *J. Geophys. Res.*, *69*, 4537.

Baker, D. N. (2000), The occurrence of operational anomalies in spacecraft and their relationship to Space Weather, *IEEE Trans. Plasma Sci.*, *28*, 2007.

Bell, T. F., U. S. Inan, J. Bortnik, and J. D. Scudder (2002), The Landau damping of magnetospherically reflected whistlers within the plasmasphere, *Geophys. Res. Lett.*, *29*(15), 1733, doi:10.1029/2002GL014752.

Bortnik, J., U. S. Inan, and T. F. Bell (2003a), Energy distribution and lifetime of magnetospherically reflecting whistlers in the plasmasphere, *J. Geophys. Res.*, *108*(A5), 1199, doi:10.1029/2002JA009316.

Bortnik, J., U. S. Inan, and T. F. Bell (2003b), Frequency-time spectra of magnetospherically reflecting whistlers in the plasmasphere, *J. Geophys. Res.*, *108*(A1), 1030, doi:10.1029/2002JA009387.

Brinca, A. L. (1981), Enhancing whistler wave-electron interaction by the use of specially modulated VLF wave injection, *J. Geophys. Res.*, *86*, 792.

Cairó, L., and F. Lefeuvre (1986), Localization of sources of ELF/VLF hiss observed in the magnetosphere: Three-dimensional ray traycing, *J. Geophys. Res.*, *91*, 4352.

Carpenter, D. L., and R. R. Anderson (1992), An ISEE/Whistler model of equatorial electron density in the magnetosphere, *J. Geophys. Res.*, *97*, 1097.

Edgar, B. C. (1972), The structure of the magnetosphere as deduced from magnetospherically reflected whistlers, *Tech. Rep. 3438-2*, Radiosci. Lab., Stanford Electron. Lab., Stanford Univ., Stanford, Calif.

Edgar, B. C. (1976), The upper and lower frequency cutoffs of magnetospherically reflected whistlers, *J. Geophy. Res.*, *81*, 205.

Gurnett, D. A., and U. S. Inan (1988), Review of plasma wave observations with Dynamics Explorer 1, *Rev. of Geophys.*, *26*, 285.

Inan, U. S. (1987), Gyroresonant pitch angle scattering by coherent and incoherent whistler mode waves in the magnetosphere, *J. Geophys. Res.*, *92*, 127.

Inan, U. S., and T. F. Bell (1977), The plasmapause as a VLF waveguide, *J. Geophys. Res.*, *82*, 2819.

Inan, U. S., T. F. Bell, J. Bortnik, and J. M. Albert (2003), Controlled precipitation of radiation belt electrons, *J. Geophys. Res.*, *108*(A5), 1186, doi:10.1029/2002JA009580.

Kennel, C. F., and H. E. Petschek (1966), Limit on stably trapped particle fluxes, *J. Geophys. Res.*, *99*, 1.

Lyons, L. R., R. M. Thorne, and C. F. Kennel (1972), Pitch angle diffusion of radiation belt electrons within the plasmasphere, *J. Geophys. Res.*, *77*, 3455.

Ristic'-Djurovic', J. L., T. F. Bell, and U. S. Inan (1998), Precipitation of radiation belt electrons by magnetospherically reflecting whistlers, *J. Geophys. Res.*, *103*, 9249.

Shklyar, D. R., and F. Jiříček (2000), Simulation of nonducted whistler spectrograms observed aboard the Magion 4 and 5 Satellites, *J. Atmos. Sol. Terr. Phys.*, *62*, 347.

Smith, R. L., and J. J. Angerami (1968), Magnetospheric properties deducted from OGO 1 observations of ducted and nonducted whistlers, *J. Geophys. Res.*, *73*, 1.

Thorne, R. M., and R. B. Horne (1994), Landau damping of magnetospherically reflected whistlers, *J. Geophys. Res.*, *99*, 17,249.

Wang, T. N. C., and T. F. Bell (1970), On the VLF/ELF radiation resistance of an electric dipole in a cold magnetoplasma, *Radio Sci.*, *5*, 605.

T. F. Bell, U. S. Inan, and P. Kulkarni, STAR Laboratory, 301 Packard Building, MC 9515, 350 Serra Mall, Stanford, CA 94305, USA. (pxk161@stanford.edu)